ChemPhysChem

Research Article
doi.org/10.1002/cphc.202200069

Chemistry Europe
European Chemical Societies Publishing

www.chemphyschem.org

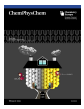

DFT Study of the BH_4^- Hydrolysis on Au(111) Surface

Basil Raju Karimadom,[a] Shalaka Varshney,[a] Tomer Zidki,[a] Dan Meyerstein,[a, b] and Haya Kornweitz*[a]

The mechanism of the catalytic hydrolysis of BH_4^- on Au(111) as studied by DFT is reported. The results are compared to the analogous process on Ag(111) that was recently reported. It is found that the borohydride species are adsorbed stronger on the Au^0-NP surface than on the Ag^0-NP surface. The electron affinity of the Au is larger than that of Ag. The results indicate that only two steps of hydrolysis are happening on the Au(111) surface and the reaction mechanism differs significantly from that on the Ag(111) surface. These remarkable results were experimentally verified. Upon hydrolysis, only three hydrogens of BH_4^- are transferred to the Au surface, not all four, and H_2 generation is enhanced in the presence of surface H atoms. Thus, it is proposed that the BH_4^- hydrolysis and reduction mechanisms catalyzed by M^0-NPs depend considerably on the nature of the metal.

Introduction

Hydrogen is considered a potential replacement for existing fossil fuel based energy systems due to its high energy content, zero pollution emission and high environmental abundance.[1–3] Researchers consider borohydride as the front runner in this research due to its cheap production and high theoretical hydrogen storage capacity (10.8 wt.%).[2,4–7] In addition to the comprehensive experimental efforts,[8–14] computational studies at various levels are also used to understand the catalyzed and uncatalyzed hydrogen evolution reaction (HER) mechanism of BH_4^- hydrolysis.[15–18] Mondal et al. studied the homogeneous catalytic hydrolysis of BH_4^- in the presence of $Ag(H_2O)_2^+$[16] and $AuCl_4^-$.[17] Escaño et al.[19–21] reported the adsorption properties of BH_4^- on metallic surfaces such as Au, Pt, Pd, Ir, Os, Mn etc. and Akça et al.[22] investigated the sequential decomposition of BH_4 on Au, Cu, Al and Ag(111) surfaces. The electro-oxidation of BH_4^- was also investigated theoretically on Au[23] and Pt(111)[15] surfaces.

In parallel to electrochemistry, HER on metal surfaces is commonly assumed to proceed via one of two mechanisms:[11,24,25]

$$\{(M^0-NP)-H_m\}^{(n-m)^-} + H^+ \rightarrow \{(M^0-NP)-H_{m+1}\}^{(n-m-1)^-} \quad \text{(Tafel)} \quad (1)$$

$$\{(M^0-NP)-H_{m+1}\}^{(n-m-1)^-} \rightarrow \{(M^0-NP)-H_{m-1}\}^{(n-m-1)^-} + H_2 \quad \text{(Tafel)} \quad (2)$$

$$\{(M^0-NP)-H_m\}^{(n-m)^-} + H^+ + H_2 \rightarrow \{(M^0-NP)-H_m\}^{(n-m-1)^-} \quad \text{(Heyrovsky)} \quad (3)$$

The metal-catalyzed hydrolysis of BH_4^- is expected to proceed via transfer of all four hydrogens to the surface upon hydrolysis.[11] However, a recent study shows that at least on Ag^0-NP this mechanism is wrong; only in the first step, one hydrogen is transferred to the surface from BH_4^- upon hydrolysis,[26] and another H_2 molecule is released in the second step. Another computational study by Mondal et al. reported that $Ag(H_2O)_2^+$ is a better catalyst than $AuCl_4^-$ for the BH_4^- hydrolysis and the formation mechanism of Ag^0-NP and Au^0-NP via Creighton process[27] differs significantly.[17] Herein are reported the results of a DFT analysis of the reaction mechanism of BH_4^- hydrolysis on Au^0-NP surface. The results demonstrate that the catalytic BH_4^- hydrolysis on the surfaces of Ag^0 and Au^0 proceed via different mechanisms. Thus, the same mechanism cannot be considered on different metals without proof, as commonly assumed. These results were experimentally verified by measuring the time-dependent H_2 evolution yields via the Ag^0-NPs & Au^0-NPs catalyzed hydrolysis of BH_4^-.

[a] B. Raju Karimadom, Dr. S. Varshney, Dr. T. Zidki, Prof. Dr. D. Meyerstein, Prof. Dr. H. Kornweitz
Chemical Science Department and The Radical Research Centre
Ariel University
P.O.B. 3 Ariel
40700, Ariel, Israel
E-mail: hayak@ariel.ac.il
[b] Prof. Dr. D. Meyerstein
Chemistry Department
Ben-Gurion University
Beer-Sheva, Israel

Supporting information for this article is available on the WWW under https://doi.org/10.1002/cphc.202200069

Experimental Section

Computational Details

The Vienna Ab-initio Simulation Package (VASP)[28,29] was used for all the DFT calculations in this work with GGA-PBE[30] exchange-correlation functional and ion cores are modeled with PAW pseudo-potentials.[31,32] The plane wave cut-off energy of 400 eV is used to describe the valence electrons and 8x8x1 Monkhosrt pack[33] k-point mesh is used for Brillouin zone integration. The climbing image nudged elastic band method (Cl-NEB)[34] is used to locate the transition state. The DFT–D2 Van der Walls correction by Grimmie[35,36] and solvent effect using VASPsol[37,38] are also considered in all calculations.

The Au(111) surface is modelled with six layers of Au, which contains eight Au atoms in each layer. To avoid the unwanted interactions between the slabs, 16 Å of vacuum thickness is introduced between the slabs in the z-direction. The counter ion (CI) method[26] is used to calculate the adsorption energy of the charged adsorbents on the surface, in this method the supercell is neutral as a counter ion is placed in a non-interacting distance, the ionic model is achieved using an implicit self-consistent electrolyte solvation model (VASPsol). The Bader charge analysis program[39] is used to verify the correct charge of the ions. The adsorption energies (E_{ads}) of the ions are calculated using the equation:

$$E_{ads} = (E^{*} + E^{s}) - E^{*s} \quad (4)$$

Where E* is the energy of the surface, E^s is the energy of the adsorbent molecule alone and E*s is the energy of the adsorbed system (surface and substrate). The phonon calculations are carried out with 0.015 Å step width to obtain the zero-point vibration energies (ZPVE) of the system, using the harmonic oscillator approximation. The reaction free energies (ΔG^0) are calculated using the equation:

$$\Delta G^{0} = [\mathbf{E} + \mathbf{ZPVE} + (\mathbf{T^{*}S})]_{Products} - [\mathbf{E} + \mathbf{ZPVE} + (\mathbf{T^{*}S})]_{Reactants}$$

Where, S is the entropy and T is the temperature (298.15 K).

Experimental Details

Materials: All chemicals were of analytical grade and were used without further purification. Silver sulfate (Ag_2SO_4), tetra-chloro-auric acid ($HAuCl_4$), and sodium borohydride ($NaBH_4$) were purchased from Strem Chemicals. Sulfuric acid (H_2SO_4) was purchased from Merck. Millipore water, with a resistivity of >15 MΩ cm, was used throughout the experiments.

Methods and Instrumentation: To follow the reaction kinetics, we used a manometer-based set-up as follows: the reactions took place in a two-neck round bottom flask reactor (50 mL); one neck of the reactor is connected via a pipe to a U-tube manometer; the other neck is closed with a rubber septum for Ar purging and reagent additions. Before the last reagent, $NaBH_4$, is added, the water level in the arms of the manometer was balanced. The hydrogen evolution kinetics was followed by reading the water level in the U-tube manometer.

Catalyst Preparation: The M^0-NPs suspensions, were prepared as reported elsewhere using the modified Creighton's procedure[27] by Zidki et al..[40–42] Briefly, 30 mL of an ice-cold aqueous solution containing $NaBH_4$ (2.0 mM) were added at once under vigorous stirring to 10 mL of 1.0 mM of the desired precursor salts dissolved in water ($HAuCl_4$, and Ag_2SO_4 for Ag and Au, respectively). The final metal ion concentration was 2.5×10^{-4} M. All the NP concentrations are stated as ion-based M^{n+} concentrations in all experiments. The resulting suspensions were yellow and ruby red for Ag and Au M^0-NPs, respectively. The M^0-NPs pH was ~9.0 due to the borate formed during the NP synthesis[43] and the borohydride hydrolysis, which acts as a buffer. Note that all the M^0-NPs have some oxides on their surface, which are partially responsible for maintaining their stability in aqueous suspensions.

Hydrogen Evolution Experiments: In a typical procedure, 50 mL of water were mixed with 2.35 mL of M^0-NPs (to give 11.2 μM as a metal ion concentration) in the reactor and purged with Ar for 15 min during stirring. The water level of the arms of the manometer was balanced before the last added reagent. Then, 0.30 mL, 0.106 M of Ar-purged, freshly prepared $NaBH_4$ (a final concentration of 6.0×10^{-4} M in the reaction) was quickly added to the reactor to initiate the catalytic reaction. All the reactions were performed at room temperature (24 °C). Note that the water level in the manometer did not change appreciably since the $NaBH_4$ solution was concentrated to allow the addition of a minimal volume of the reagents. As the reaction proceeded, the water level in the manometer was recorded at different time intervals, providing the hydrogen evolution rate for each catalyst. The resulting data are plotted as hydrogen yield vs. time. The calculated amount of H_2 from the complete conversion of $NaBH_4$ to hydrogen is 126.36 μmol, resulting in 100% H_2 yield and a gauge pressure of 479 Pa (calculated using the ideal gas equation). This value is denoted in the figure by a dashed line. The hydrogen yield was calculated accordingly from three independent measurements for each data point and the graphs have an experimental error limit value of ±5%.

Results and Discussion

Molecular Adsorption on Au(111)

Au bulk has a fcc structure;[45,46] therefore, Au(111) surface has four adsorption sites: atop, bridge, fcc hollow and hcp hollow. The optimized ground state geometries of various species involved in BH_4^- hydrolysis adsorbed on Au(111) surface are given in Figure 1 and the adsorption energies, charge transfer, and binding distances are tabulated in Table 1. The adsorption energies of the neutral species that are given in Table 1 are higher than those published earlier, given as a footnote in table1, due to the different computational details. These values do not include the ZPVE correction, they are calculated using solvent effects and not vacuum, dispersion is taken into account, the adsorption sites may be different, and the coverage ratio is small (0.125).

The species formed during the BH_4^- hydrolysis reactions are better adsorbed on Au(111) surface than on the Ag(111) surface. Both surfaces have similar adsorption sites, and the extent of adsorption linearly depends on the amount of charge transferred to the surface from the adsorbates. BH_4^- and $BH_n(OH)_{4-n}^-$ species (where n = 0,1,2,3) were adsorbed on fcc-top, where boron is in the middle of the fcc site and the H and the O atoms are on the top sites of Au and Ag. The H_2O molecule is adsorbed on the Au atop position via the oxygen atom, while it is adsorbed via H atoms to the Au surface when

Table 1. Adsorption energies, charge transfer and binding distances of each species in BH_4^- hydrolysis on Au(111) and Ag(111) surface.

Adsorbate	Adsorption Site	Au(111) Adsorption Energy [eV]	Charge Transfer [$\bar{e}$][a]	Au–H Distance [Å]	Au–O Distance [Å]	Ag(111)[26] Adsorption Energy [eV]	Charge Transfer [$\bar{e}$][a]	Ag–H Distance [Å]	Ag–O Distance [Å]
H^-	fcc	2.96	−0.85	1.80	–	2.32	−0.67	1.80	–
H	fcc	3.30[b]	0.10	1.80	–	3.19[b]	0.27	1.80	–
H_2	atop	0.01	-0.02	2.24	–	0.09	−0.02	2.40	–
H_2O	atop	0.39[b]	−0.08	2.86	2.49	0.31	−0.03	2.80	2.50
BH_4^-	fcc	1.26	−0.53	1.94	–	0.91	−0.30	2.00	–
BH_3	fcc	1.34[b]	0.13	2.03	–	1.11[b]	0.40	2.15	–
$BH_3(OH)^-$	fcc	1.60	−0.52	1.94	2.51	1.12	−0.32	1.90	2.40
$BH_2(OH)_2^-$	fcc	1.59	−0.41	2.13	2.40	1.10	−0.25	2.10	2.30
$BH(OH)_2$	fcc	0.63	−0.01	2.79	2.95	0.21	0.09	2.60	3.10
$BH(OH)_3^-$	fcc	1.64	−0.40	–	2.43	1.22	−0.26	–	2.30

[a] A Negative value indicates charge transfer from adsorbate to the surface, and a positive value indicates charge transfer from the surface to the adsorbate. [b] Adsorption energies according to ref. 22: 0.86 eV for BH_3/Au(111) and 0.82 eV for BH_3/Ag(111), 2.12 eV for H/Au(111) and 0.11 for H2O/Au(111). according to ref. 44: 2.21 eV for H/Ag(111)

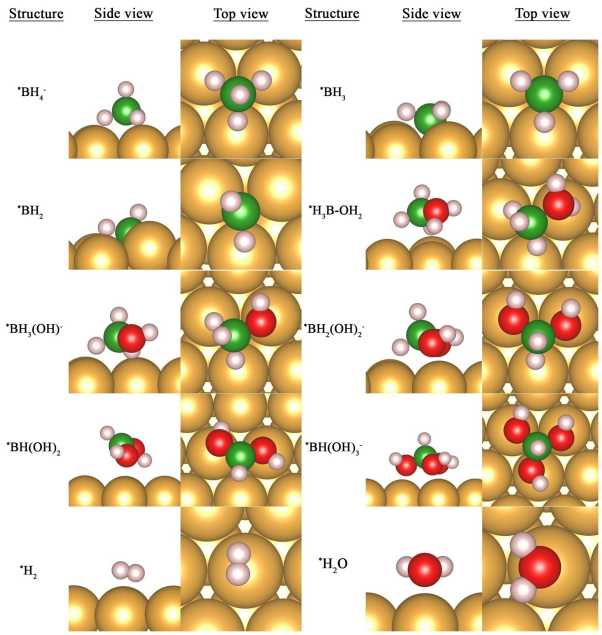

Figure 1. Optimized ground state adsorption geometries of various species on Au(111) surface.

co-adsorbed with BH_4^- and $BH_n(OH)_{4-n}^-$ species, similar to the reported configuration on Ag(111).[26]

Dissociation Mechanism of BH_4^- on Au(111)

The DFT studies of Akça et al.[22] reported sequential decomposition of BH_4 on various metal surfaces. Their study showed that Au(111) surface is kinetically favored over Ag(111) surface for the dissociation of BH_4 to BH_3 and H on the metal surface even though the dissociation is thermodynamically unfavorable. Since their calculations did not account for the charges on the adsorbed species, it should be reassessed with the charged ions.

On Au(111) surface the BH_4^- dissociate as follows (*X means that X is adsorbed at the surface);

$$^*BH_4^- \rightarrow {}^*BH_3 + {}^*H + {}^*\bar{e} \quad (5)$$

$$\Delta G^0 = -0.02\ eV\ (E_a = 0.72\ eV)$$

$$^*BH_3 \rightarrow {}^*BH_2 + {}^*H \quad (6)$$

$$\Delta G^0 = 0.37\ eV$$

Reaction (5) is thermodynamically and kinetically feasible on Au(111) surface but it is thermodynamically unfavored on Ag(111) surface ($\Delta G^0 = 0.42$ eV) and the dissociation is not observed on the Ag surface. According to reaction (5), BH_4^- dissociates and transfers its charge to the Au(111) surface, while BH_3 is adsorbed as a radical on the Au surface (surface charge is $-0.61\bar{e}$). The subsequent dissociation of BH_3 to BH_2 is highly endothermic on Au(111) (reaction *(6)*), so only one hydrogen is transferred to the surface from BH_4^- upon dissociation. TSn denotes the transition state (TS) of reaction n, and all relevant TS geometries are given in Figure 2.

Hydrolysis of BH_4^- on the Au(111) surface

Spectroscopic[8,14] and computational[16,26] studies suggest a sequential four-step reaction mechanism for the hydrolysis of BH_4^- (Scheme 1). In this section, the four-step hydrolysis mechanism is explored on Au(111) surface to account for the kinetic and thermodynamic feasibilities of each step.

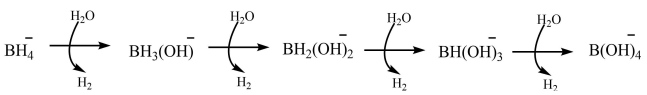

Scheme 1. Reaction channel of BH_4^- hydrolysis.

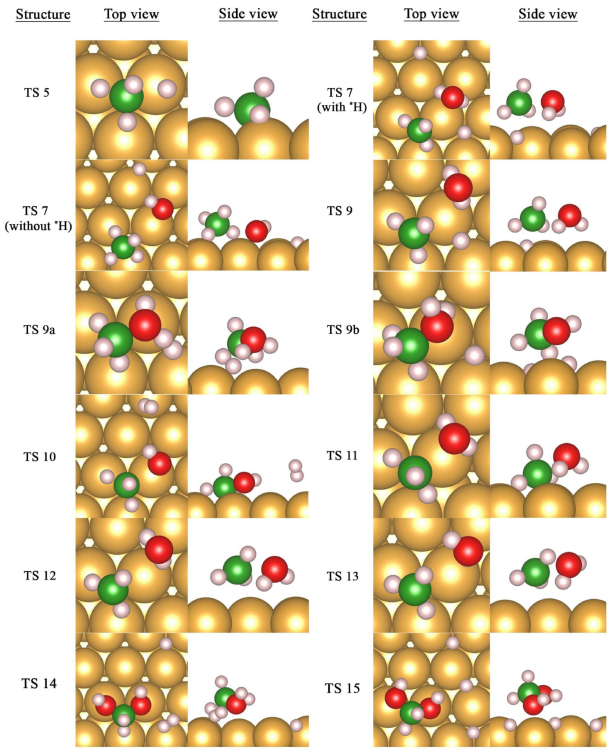

Figure 2. TS geometries of each step of BH_4^- hydrolysis on Au(111) surface.

First Step: The existence of short-lived $BH_3(OH)^-$ is observed experimentally[8] during the hydrolysis of BH_4^-. The $BH_3(OH)^-$ species is formed along with either H_2 or H atoms.

$$^*BH_4^- + {}^*H_2O \rightarrow {}^*BH_3(OH)^- + {}^*2H \quad (7)$$

$$\Delta G^0 = -0.28\ eV\ (E_a = 1.72\ eV;\ 0.89\ eV\ in\ the\ presence\ of\ {}^*H)$$

The activation energy barrier for hydrogen atoms formation on the Au(111) surface is significantly larger than that on the Ag^0 surface (0.99 eV).[26] Recent experimental studies have shown that the pre-adsorbed H on Au^0-NP surface affects its electronic structures[47] and for the hydrolysis BH_4^-, M^0-NPs–H is the starting point.[11] The presence of H changes the TS geometry of reaction (7) (Figure 2) and Au^0 surface becomes more negative (surface charge −0.68 $\bar{e}$) while in the absence of H on the surface it is neutral (surface charge = +0.06 $\bar{e}$).

$$^*BH_4^- + {}^*H_2O \rightarrow {}^*BH_3(OH)^- + {}^*H_2 \quad (8)$$

$$\Delta G^0 = -0.23\ eV$$

According to the NEB analysis of reaction (8), BH_4^- forms a stable intermediate, H_3B-OH_2 on the surface by transferring one hydrogen from BH_4^- to the surface.

$$^*BH_4^- + {}^*H_2O \rightarrow {}^*H_3B-OH_2 + {}^*H + {}^*\bar{e} \quad (9)$$

$$\Delta G^0 = -0.28\ eV\ (E_a = 0.92\ eV)$$

Thus, it opens a new pathway for the formation of $BH_3(OH)^-$ compared to the reaction mechanism on the Ag^0 surface.

$$^*H_3B-OH_2 + {}^*H + {}^*\bar{e} \rightarrow {}^*BH_3(OH)^- + {}^*H_2 \quad (9a)$$

$$\Delta G^0 = 0.05\ eV\ (E_a = 0.25\ eV)$$

$$^*H_3B-OH_2 + {}^*H + {}^*\bar{e} \rightarrow {}^*BH_3(OH)^- + {}^*2H \quad (9b)$$

$$\Delta G^0 = 0.00\ eV\ (E_a = 0.58\ eV)$$

The H_3B-OH_2 intermediate enhances the H_2 formation on the Au^0 surface compared to the hydrogen atom release to the surface. However, the activation energy barrier of reaction (9) is significantly higher than reaction (5) and BH_3 formation on the Au surface is preferred. Since reaction (6) is highly endothermic, BH_3 will react with water according to one of the following reactions:

$$^*BH_3 + {}^*H_2O + {}^*H + {}^*\bar{e} \rightarrow {}^*BH_3(OH)^- + {}^*H_2 \quad (10)$$

$$\Delta G^0 = -0.21\ eV\ (E_a = 2.26\ eV)$$

$$^*BH_3 + {}^*H_2O + {}^*\bar{e} \rightarrow {}^*BH_3(OH)^- + {}^*H \quad (11)$$

$$\Delta G^0 = -0.18\ eV\ (E_a = 1.14\ eV;\ 0.99\ eV\ in\ the\ presence\ of\ {}^*H)$$

$$^*BH_3 + {}^*H_2O + {}^*\bar{e} \rightarrow {}^*H_3B-OH_2 + {}^*\bar{e} \quad (12)$$

$$\Delta G^0 = -0.26\ eV\ (E_a = 0.74\ eV;\ 0.73\ eV\ in\ the\ presence\ of\ {}^*H)$$

The formation of the H_3B-OH_2 intermediate is the thermodynamically and kinetically favored step of the reaction between BH_3 and H_2O. Since the surface is charged, presence of the adsorbed H on the surface is less significant in reactions (11) and (12). A plausible alternative to reaction (12) is the analogous reaction with a water molecule not adsorbed on the surface:

$$^*BH_3 + H_2O_{(aq)} + {}^*\bar{e} \rightarrow {}^*H_3B-OH_2 + {}^*\bar{e} \quad (13)$$

$$\Delta G^0 = -0.46\ eV\ (E_a = 0.62\ eV)$$

Reaction (13) is clearly favored over reaction (12). Reactions (8) and (11) were also reassessed with an aqueous water molecule reacting with the adsorbed species (S1 and S2); however, these reactions are kinetically un-favorable due to the large activation energy barriers. In contrast with the hydrolysis mechanism on Ag(111) surface, $BH_3(OH)^-$ formation on Au(111) surface is a multi-step process with an aqueous water molecule instead of the one-step process with adsorbed water molecule on Ag(111).[26] Due to this multi-step process on Au^0-NPs, the H_2 generation will be slower than that on the Ag^0-NPs. The reaction profile is given in Figure 3 and Scheme 2.

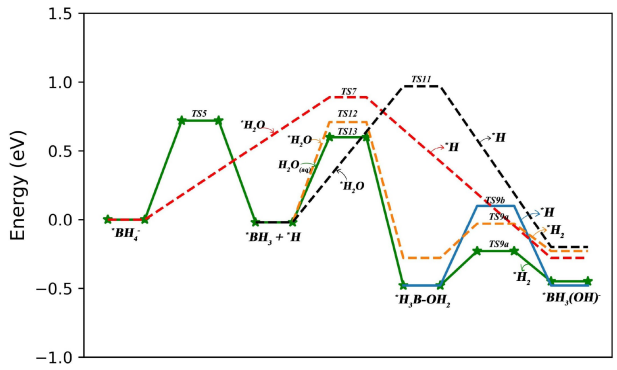

Figure 3. Relative Gibbs free energy change (ΔG^0) for the intermediates and TS involved in the first step of BH_4^- hydrolysis on Au(111) surface.

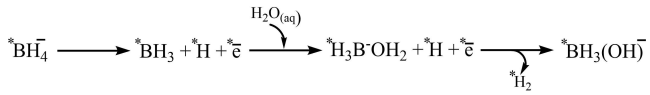

Scheme 2. Reaction pathway for the formation of $BH_3(OH)^-$ on Au(111).

Second Step: $BH_2(OH)_2^-$ is formed on the Au(111) surface via:

$$^{*}\mathbf{BH_3(OH)^-} + {}^{*}\mathbf{H_2O} \rightarrow {}^{*}\boldsymbol{BH_2(OH)_2^-} + {}^{*}\boldsymbol{H_2} \quad (14)$$

$\Delta G^0 = -0.15\ eV\ (E_a = 1.30\ eV;\ 0.48\ eV\ in\ the\ presence\ of\ {}^{*}H)$

$$^{*}\mathbf{BH_3(OH)^-} + {}^{*}\mathbf{H_2O} \rightarrow {}^{*}\boldsymbol{BH_2(OH)_2^-} + {}^{*}\boldsymbol{2H} \quad (15)$$

$\Delta G^0 = -0.13\ eV\ (E_a = 0.69\ eV;\ 0.62\ eV\ in\ the\ presence\ of\ {}^{*}H)$

The second step of hydrolysis is highly dependent on the presence of H atom on the Au surface. In the absence of H on the Au surface, two hydrogen atoms are released to the surface, one from $BH_3(OH)^-$ and the other from H_2O (reaction (15)). However, in the presence of an H atom, H_2 is formed on the surface along with $BH_2(OH)_2^-$ with a lower activation energy barrier (reaction (14)). Thus, the reaction begins with the formation of hydrogen atoms on the surface afterwards, the second step proceeds via reaction (14), and an H_2 molecule is released to the surface. Reaction (14) was also evaluated for the reaction with a non-adsorbed water molecule. The latter reaction is kinetically unfavored due to a large activation energy barrier (S3). Similar to the hydrolysis mechanism on Ag(111) surface,[26] adsorbed H present on the catalyst surface enhances the H_2 generation upon hydrolysis.

Third Step: The sequential hydrolysis mechanism expects the formation of $BH(OH)_3^-$ on the Au(111) surface. The NEB study of the reaction between $BH_2(OH)_2^-$ and H_2O showed the formation of a stable $BH(OH)_2$ intermediate on the surface before the hydrolysis.

$$^{*}\mathbf{BH_2(OH)_2^-} \rightarrow {}^{*}\mathbf{BH(OH)_2} + {}^{*}\mathbf{H} + {}^{*}\mathbf{\bar{e}} \quad (16)$$

$\Delta G^0 = -1.01\ eV\ (E_a = 0.03\ eV)$

The $BH(OH)_2$ intermediate formation is highly exothermic and the H is released to the Au(111) surface without an activation energy barrier similar to that on the Ag(111) surface.[26]

$$^{*}\mathbf{BH(OH)_2} + {}^{*}\mathbf{H_2O} + {}^{*}\mathbf{H} + {}^{*}\mathbf{\bar{e}} \rightarrow {}^{*}\mathbf{BH(OH)_3^-} + {}^{*}\mathbf{H_2} \quad (17)$$

$\Delta G^0 = 0.50\ eV$

$$^{*}\mathbf{BH(OH)_2} + {}^{*}\mathbf{H_2O} + {}^{*}\mathbf{\bar{e}} \rightarrow {}^{*}\mathbf{BH(OH)_3^-} + {}^{*}\mathbf{H} \quad (18)$$

$\Delta G^0 = 0.53\ eV$

$$^{*}\mathbf{BH(OH)_2} + \mathbf{H_2O_{(aq)}} + {}^{*}\mathbf{H} + {}^{*}\mathbf{\bar{e}} \rightarrow {}^{*}\mathbf{BH(OH)_3^-} + {}^{*}\mathbf{H_2} \quad (19)$$

$\Delta G^0 = 0.30\ eV$

The hydrolysis of $BH(OH)_2$ on Au(111) surface is highly endothermic. Therefore, the formation of $BH(OH)_3^-$ and $B(OH)_4^-$ species are not observed on Au(111) surface in contrast to the results on Ag(111) surface. Hence, only two steps of hydrolysis of BH_4^- can happen on the Au(111) surface, and $BH(OH)_2$ is the final product adsorbed on the Au^0-NP surface.

The release of products from the Au(111) surface was studied according to equations (S4)–(S15). When BH_4^- is adsorbed with $BH_3(OH)^-$ and $BH_2(OH)_2^-$, BH_4^- is preferably released from the Au^0-NP surface (S4–S7). When $BH_3(OH)^-$ and $BH_2(OH)_2^-$ are adsorbed, the release of $BH_2(OH)_2^-$ is preferred (S8 and S9). However, reaction (16) is more exothermic than reaction (S9), and the H release to the Au^0-NP surface will be preferred over $BH_2(OH)_2^-$ desorption from the Au^0-NP surface. According to reactions (S10)–(S13), the $BH(OH)_2$ desorption is highly endothermic when $BH(OH)_2$ is adsorbed with other borohydride species on the Au^0-NP surface. At higher surface coverage, weakening of adsorption is observed for the adsorbates, facilitating the desorption of adsorbates from the surface.[26] The $BH(OH)_2$ adsorption energy on Au(111) surface is lowered with an increase of surface coverage (Table S1), and according to reactions (S14) and (S15), the desorption free energies of $BH(OH)_2$ from the Au^0-NP surface becomes less endothermic with increased surface coverage. Therefore, upon BH_4^- hydrolysis on Au(111) surface, $BH(OH)_2$ will be released to the aqueous phase only at a high BH_4^- coverage ratio.

The hydrogen atoms released to the surface react to form H_2 according to reaction (20) on Au^0-NP and reaction (21) on Ag^0-NP. Reaction (21) is much more exothermic (−0.30 eV) than reaction (20) (−0.03 eV). Consequently, on Au^0-NP, not all the hydrogen atoms form H_2 molecules, as reaction (20) describes an equilibrium process, while on Ag^0-NP, all the released hydrogen atoms form H_2 molecules.

$$\boldsymbol{Au(111)\ surface}: \quad {}^{*}\mathbf{2H} \rightarrow {}^{*}\mathbf{H_2} \quad (20)$$

$$\Delta G^0 = -0.03\ eV\ (E_a = 0.60\ eV)$$

$$Ag(111)\ surface: \quad {}^*2H \rightarrow {}^*H_2 \qquad (21)$$

$$\Delta G^0 = -0.30\ eV\ (E_a = 0.72\ eV)$$

The hydrolysis of BH_4^- on Ag^0-NPs and Au^0-NPs are different in their final desorbed products from the surface. In both cases the hydrolysis of BH_4^- on the surface is not complete. On the silver surface the $BH_2(OH)_2^-$ is released to the aqueous phase, as the following hydrolysis steps have a higher barrier, while $BH(OH)_2$ is the final product of hydrolysis of BH_4^- on Au^0-NP. The overall hydrolysis pathway on Ag^0-NP and Au^0-NP surface is given in Figure 4. The desorption of $BH(OH)_2$ from Au^0-NPs is endothermic and may succeed only in a very high coverage ratio. It was decided to check this conclusion experimentally.

Experimental Determination of the H_2 Yield in the Catalytic Hydrolysis of BH_4^- on Ag^0-NPs and Au^0-NPs

The kinetics of hydrogen evolution from the catalytic hydrolysis of $NaBH_4$ was investigated in the presence of Ag^0-NPs and Au^0-NPs, Figure 5. The results clearly point out that:

1. The yield of H_2 formed in the catalytic hydrolysis of BH_4^- on Ag^0-NPs and Au^0-NPs differs considerably. The experimental results are in agreement with the DFT derivation: Thus, for silver the DFT evaluation suggests that the catalysis on the surface involves 50% of the expected H_2 and then $BH_2(OH)_2^-$ is released to the aqueous phase which is expected to release the rest of the H_2 upon acid addition, in reasonable agreement with the experimental result. On the other hand, the DFT predicts that on gold $BH(OH)_2$ is the final product that does not desorb from the surface. This probably inhibits some BH_4^- from reaching the surface. This BH_4^- reacts with the acid upon addition. Why the adsorbed $BH(OH)_2$ does not react with the acid is not clear at present.
2. When H_2SO_4 is added to lower the suspension's pH to 2.0 after the catalytic process completion, the H_2 yield increases. The increment in yield reaches 100 and 60% in the Ag and Au systems, respectively. It is tentatively proposed that the acid hydrolyses the borane species released into the homogeneous aqueous phase. This suggestion is in reasonable agreement with the DFT suggestions. However, it is difficult to explain how such large amounts of $BH(OH)_2$ are adsorbed on the Au^0-NPs.

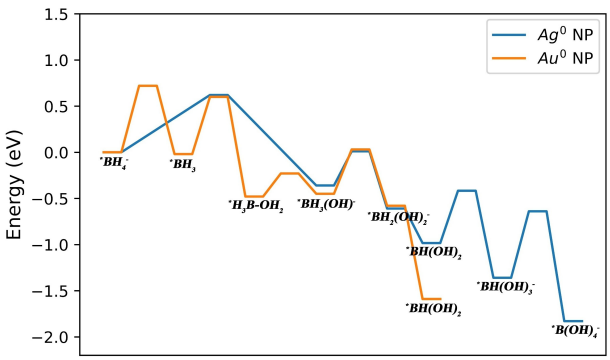

Figure 4. Relative Gibbs free energy change (ΔG^0) for the overall BH_4^- hydrolysis on Ag(111) and Au(111) surface. (Ag(111) data is reproduced from Ref. 26)

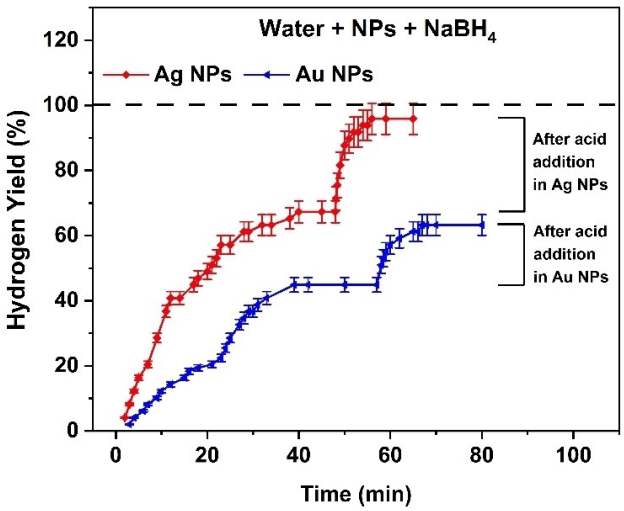

Figure 5. Hydrogen evolution kinetics from $NaBH_4$ hydrolysis on Ag and Au, M^0-NPs. In water, the Initial pH was neutral, and the pH after the reaction completion was 9.3; 11.2 μM NPs (ion-based concentration); 0.60 mM $NaBH_4$; room temperature (24 °C).

The HER study by Sermiagin et al.[11] on the hydrolysis of BD_4^- on Ag^0-NPs and Au^0-NPs pointed out that the hydrogen evolution mechanism differs on these metals. The considerably higher HD formation on Ag^0-NPs than on Au^0-NPs is probably due to the fact that on Ag^0-NPs four H_2 molecules are released (two from the surface and two probably in the aqueous phase) whereas on Au^0-NPs only two are released.

Conclusions

The BH_4^- hydrolysis mechanism on Au(111) surface is explored computationally using DFT methods; the results are supported experimentally. The adsorption energies of the species involved in the hydrolysis reaction are considerably larger on Au(111) than on Ag(111) due to the larger charge transfer between the adsorbate and the surface. The hydrolysis begins with the dissociation of BH_4^- into BH_3 and H on the Au^0-NP surface. Upon hydrolysis, three hydrogen atoms are transferred from BH_4^- to the Au^0-NP surface instead of one hydrogen on the Ag^0-NP surface (reactions (5), (15) and (16)) and the presence of hydrogen atoms enhances the H_2 formation on the Au^0-NP surface (reaction (14)). Only two steps of hydrolysis occur on the Au^0-NP surface and $BH(OH)_2$ is the final product. The $BH(OH)_3^-$ formation is highly endothermic in contrast to the observations on the Ag^0-NP surface. Different hydrolysis products were experimentally desorbed from Ag^0- and Au^0- NPs. Not all four hydrogens of BH_4^- are catalytically hydrolyzed on the

Au^0-NP surface due to diverge hydrolysis mechanism on Au^0- and Ag^0-NPs, excluding the assumption that the catalytic BH_4^- hydrolysis mechanism on M^0-NPs is independent of the nature of M. This conclusion is probably correct also for M^0-NPs catalyzed reductions by BH_4^-.

Acknowledgements

B.R.K. and S.V is thankful to Ariel University for a Ph.D. fellowship

Conflict of Interest

The authors declare no conflict of interest.

Data Availability Statement

The data that support the findings of this study are available in the supplementary material of this article.

Keywords: hydrolysis · hydrides · gold · density functional calculations · heterogeneous catalysis

[1] F. Dawood, M. Anda, G. M. Shafiullah, *Int. J. Hydrogen Energy* **2020**, *45*, 3847–3869.
[2] H. N. Abdelhamid, *Int. J. Hydrogen Energy* **2021**, *46*, 726–765.
[3] M. Dresselhaus, G. Crabtree, M. Buchanan, T. Mallouk, L. Mets, K. Taylor, P. Jena, F. DiSalvo, T. Zawodzinski, H. Kung, I. S. Anderson, P. Britt, L. Curtiss, J. Keller, R. Kumar, W. Kwok, J. Taylor, J. Allgood, B. Campbell, K. Talamini, *Basic Research Needs for the Hydrogen Economy. Report of the Basic Energy Sciences Workshop on Hydrogen Production, Storage and Use, May 13–15, 2003*, **2004**.
[4] H. I. Schlesinger, H. C. Brown, A. E. Finholt, J. R. Gilbreath, H. R. Hoekstra, E. K. Hyde, *J. Am. Chem. Soc.* **1953**, *75*, 215–219.
[5] Ç. Çakanyıldırım, M. Gürü, *Int. J. Hydrogen Energy* **2008**, *33*, 4634–4639.
[6] S. Amendola, *Int. J. Hydrogen Energy* **2000**, *25*, 969–975.
[7] S. Choi, Y. Jeong, J. Yu, *Catal. Commun.* **2016**, *84*, 80–84.
[8] J. Andrieux, U. B. Demirci, J. Hannauer, C. Gervais, C. Goutaudier, P. Miele, *Int. J. Hydrogen Energy* **2011**, *36*, 224–233.
[9] Y.-C. Lu, M.-S. Chen, Y.-W. Chen, *Int. J. Hydrogen Energy* **2012**, *37*, 4254–4258.
[10] C. Xiang, D. Jiang, Z. She, Y. Zou, H. Chu, S. Qiu, H. Zhang, F. Xu, C. Tang, L. Sun, *Int. J. Hydrogen Energy* **2015**, *40*, 4111–4118.
[11] A. Sermiagin, D. Meyerstein, R. Bar-Ziv, T. Zidki, *Angew. Chem. Int. Ed.* **2018**, *57*, 16525–16528; *Angew. Chem.* **2018**, *130*, 16763–16766.
[12] A. Zabielaitė, A. Balčiūnaitė, I. Stalnionienė, S. Lichušina, D. Šimkūnaitė, J. Vaičiūnienė, B. Šimkūnaitė-Stanynienė, A. Selskis, L. Tamašauskaitė-Tamašiūnaitė, E. Norkus, *Int. J. Hydrogen Energy* **2018**, *43*, 23310–23318.
[13] Y. Kojima, K. I. Suzuki, K. Fukumoto, M. Sasaki, T. Yamamoto, Y. Kawai, H. Hayashi, *Int. J. Hydrogen Energy* **2002**, *27*, 1029–1034.
[14] G. Guella, B. Patton, A. Miotello, *J. Phys. Chem. C* **2007**, *111*, 18744–18750.
[15] G. Rostamikia, M. J. Janik, *Electrochim. Acta* **2010**, *55*, 1175–1183.
[16] T. Mondal, A. Sermiagin, D. Meyerstein, T. Zidki, H. Kornweitz, *Nanoscale* **2020**, *12*, 1657–1672.
[17] T. Mondal, A. Sermiagin, T. Zidki, A. Bogot, D. Meyerstein, H. Kornweitz, *J. Phys. Chem. A* **2020**, *124*, 10765–10776.
[18] Y. Zhou, C. Fang, Y. Fang, F. Zhu, H. Liu, H. Ge, *Int. J. Hydrogen Energy* **2016**, *41*, 22668–22676.
[19] M. C. S. Escaño, E. Gyenge, R. L. Arevalo, H. Kasai, *J. Phys. Chem. C* **2011**, *115*, 19883–19889.
[20] M. C. S. Escaño, R. L. Arevalo, E. Gyenge, H. Kasai, *Catal. Sci. Technol.* **2014**, *4*, 1301–1312.
[21] R. L. Arevalo, M. C. S. Escãno, H. Kasai, *e-Journal Surf. Sci. Nanotechnol.* **2011**, *9*, 257–264.
[22] A. Akça, A. E. Genç, B. Kutlu, *Appl. Surf. Sci.* **2019**, *473*, 681–692.
[23] G. Rostamikia, M. J. Janik, *J. Electrochem. Soc.* **2009**, *156*, B86.
[24] G. S. Rolly, A. Sermiagin, D. Meyerstein, T. Zidki, *Eur. J. Inorg. Chem.* **2021**, *2021*, 3054–3058.
[25] Y. Wang, W. Qiu, E. Song, F. Gu, Z. Zheng, X. Zhao, Y. Zhao, J. Liu, W. Zhang, *Natl. Sci. Rev.* **2018**, *5*, 327–341.
[26] B. R. Karimadom, D. Meyerstein, H. Kornweitz, *Phys. Chem. Chem. Phys.* **2021**, *23*, 25667–25678.
[27] J. A. Creighton, C. G. Blatchford, M. G. Albrecht, *J. Chem. Soc. Faraday Trans. 2* **1979**, *75*, 790.
[28] G. Kresse, J. Hafner, *Phys. Rev. B* **1993**, *47*, 558–561.
[29] G. Kresse, J. Furthmüller, *Phys. Rev. B: Condens. Matter Mater. Phys.* **1996**, *54*, 11169–11186.
[30] J. P. Perdew, K. Burke, M. Ernzerhof, *Phys. Rev. Lett.* **1996**, *77*, 3865–3868.
[31] D. Joubert, *Phys. Rev. B: Condens. Matter Mater. Phys.* **1999**, *59*, 1758–1775.
[32] N. Holzwarth, G. Matthews, R. Dunning, A. Tackett, Y. Zeng, *Phys. Rev. B: Condens. Matter Mater. Phys.* **1997**, *55*, 2005–2017.
[33] H. J. Monkhorst, J. D. Pack, *Phys. Rev. B* **1976**, *13*, 5188–5192.
[34] G. Henkelman, B. P. Uberuaga, H. Jónsson, *J. Chem. Phys.* **2000**, *113*, 9901–9904.
[35] S. Grimme, *J. Comput. Chem.* **2006**, *27*, 1787–1799.
[36] S. Grimme, J. Antony, S. Ehrlich, H. Krieg, *J. Chem. Phys.* **2010**, *132*, 154104.
[37] M. Fishman, H. L. Zhuang, K. Mathew, W. Dirschka, R. G. Hennig, *Phys. Rev. B: Condens. Matter Mater. Phys.* **2013**, *87*, 245402.
[38] K. Mathew, R. Sundararaman, K. Letchworth-Weaver, T. A. Arias, R. G. Hennig, *J. Chem. Phys.* **2014**, *140*, 084106.
[39] W. Tang, E. Sanville, G. Henkelman, *J. Phys. Condens. Matter* **2009**, *21*, 84204–84211.
[40] S. Varshney, R. Bar-Ziv, T. Zidki, *ChemCatChem* **2020**, *12*, 4680–4688.
[41] G. Benjamini, R. Bar-Ziv, T. Zidki, E. J. C. Borojovich, G. Yardeni, H. Kornweitz, D. Meyerstein, *Eur. J. Inorg. Chem.* **2017**, *2017*, 3655–3660.
[42] T. Zidki, H. Cohen, D. Meyerstein, *Phys. Chem. Chem. Phys.* **2010**, *12*, 12862–12867.
[43] R. Bar-Ziv, I. Zilbermann, T. Zidki, G. Yardeni, V. Shevchenko, D. Meyerstein, *Chem. A Eur. J.* **2012**, *18*, 6733–6736.
[44] A. Montoya, A. Schlunke, B. S. Haynes, *J. Phys. Chem. B* **2006**, *110*, 17145–17154.
[45] E. A. Owen, E. L. Yates, *London, Edinburgh, Dublin Philos. Mag. J. Sci.* **1933**, *15*, 472–488.
[46] L. P. Salamakha, E. Bauer, S. I. Mudryi, A. P. Gonçalves, M. Almeida, H. Noël, *J. Alloys Compd.* **2009**, *479*, 184–188.
[47] R. Ishida, S. Hayashi, S. Yamazoe, K. Kato, T. Tsukuda, *J. Phys. Chem. Lett.* **2017**, *8*, 2368–2372.

Manuscript received: January 27, 2022
Revised manuscript received: April 10, 2022
Accepted manuscript online: April 11, 2022
Version of record online: May 17, 2022